RSC Advances

ROYAL SOCIETY OF CHEMISTRY

www.rsc.org/advances

Journal Name

RSCPublishing

ARTICLE

Self-healable castor oil based tough smart hyperbranched polyurethane nanocomposite with antimicrobial attribute

Suman Thakur, Shaswat Barua and Niranjan Karak*

Cite this: DOI: 10.1039/xoxxoooooox

Received ooth January 2012,
Accepted ooth January 2012

DOI: 10.1039/xoxxoooooox

www.rsc.org/

Here, castor oil based tough hyperbranched polyurethane/sulfur nanoparticles decorated reduced graphene oxide (HPU/SRGO) nanocomposites are fabricated with different weight% of nanohybrid. Tremendous enhancement of mechanical properties such as tensile strength (from 7.2 to 24.3 MPa), tensile modulus (from 3.3 to 137.7 MPa), toughness (from 25.4 to 313.52 MJm-3) and elongation at break (from 710 to 1456%) are observed upon incorporation of nanohybrid in HPU matrix due to strong interaction between SRGO and HPU matrix. The nanocomposite exhibited excellent repeatable self-healing (within 50-60s at 360W under microwave and 5-7.5 min under sunlight) and shape recovery (within 30-50s at 360W under microwave and 1-3 min under sunlight). The nanocomposite also demonstrated profound microbial inhibitory effect against *Staphylococcus aureus*, *Escherichia coli* and *Candida albicans*. Thus, the studied nanocomposite has tremendous potential for various advanced applications.

INTRODUCTION

Recent time, an immense interest is paid to develop self-healing materials which can repair their damages by using inherent nature of the materials.[1-3] The self-healing capability of material helps to extend their service period, facilitates their maintenance and increases their reliability.[4] Recently, most of the self-healing materials are being developed based on encapsulation and reversible chemistry, with covalent and noncovalent chemical bonds.[5-14] The encapsulation approach is achieved by incorporation of microcapsules containing healing agent, which readily polymerizes in the damaged area upon release from the microcapsules.[5,6] Although the approach has a great potential for internally healing but fails to heal a macroscopic damage. In addition, the irreversible healing nature is another inadequacy of it. The last limitation can be overcome by use of reversible chemistry.[7] Intermolecular interactions and reversible bonds have been demonstrated to be particularly useful to introduce the ability to heal a polymer for multiple times. At this juncture, it is important to mention that a new concept is developed that uses shape memory materials for improvement of the self-healing process.[15] These shape memory materials are provided a mechanism to partially or fully close the crack and helps to repair it. Rowan and his coworkers prepared a polymer with a structurally dynamic polydisulfide networks which exhibited both shape memory and self-healing properties.[16] They proposed that shape memory behavior of the polymer helps in the healing process by bringing crack surfaces into close proximity. Zhao also reported that cross-linked polyethylene/carbon black nanocomposites exhibited improved self-healing by shape memory effect (SME).[17] Bai and his team recently prepared a poly(vinyl butyral) based polymer which also demonstrated both self-healing and SME.[18] Shape memory polymers (SMP) have capability to recover the original shape from a temporary deformed shape upon exposure to an external stimulus like thermal energy, electricity, magnetic field, light etc.[19-22] Structurally, SMP are usually composed of hard and soft segment.[23] The hard segment is physically or chemically cross-linked structure that controls permanent shape and soft segment is generally crystalline or amorphous part of the polymer which is mainly responsible for the shape fixity.[24] Many polymers possess SME but polyurethanes (PU) demonstrate themselves as one of the most promising SMPs among them. This is due to their high recoverable strain (up to 400%), wide range of transition temperature for their shape recovery, high control on the softening and retraction temperatures, inherent soft-hard segments, favorable and tunable physical properties etc.[25]

In this context, vegetable oil-based shape memory PU are in high demand due to global scientific community trust to opt for renewable bioresources endowing green credentials. Castor oil is one of the best industrially used vegetable oils for unique

fatty acid composition (92-95% ricinoleic acid) and easy availability.[26] It is pertinent to mention that monoglyceride of castor oil is better choice as a triol compared to oil itself in the synthesis of hyperbranched polyurethane.[27] Hyperbranched polymer curved a distinct interest over its linear counterpart due to unusual and desirable properties.[28] Further, Huang and his coworkers reported that polyurethane/graphene nanocomposite exhibited multi-stimuli responsive self-healing behavior for multiple times.[29] In this context, reduced graphene oxide (RGO) has some functional groups on its surface which help to better dispersion compared to graphene in the polymer matrix.[30] RGO also have excellent thermal conductivity, microwave (MW) and sunlight absorbing capacity almost equivalent to graphene.

Again, sulfur containing compounds and polysulfanes show significant potential as antimicrobial agents.[31] Furthermore, RGO and sulfur nanoparticles both individually exhibited good antimicrobial activity.[31,32] Microbial contaminations or infections are severe threats to mankind. Various environmental factors lead to the fouling of polymeric materials. Microbial fouling is the vital force that causes degradation of polymeric materials in due course of time. Interestingly, vegetable oil based polyurethane exhibited biodegradability on exposure to different microbes.[33] Keeping this in mind, it is desired to fabricate polymers with repeated healing capability, excellent shape recovery along with antibacterial attributes for different avant-grade applications. Therefore, sulfur nanoparticles decorated RGO (SRGO) nanohybrid may be a right choice to prepare antimicrobial polymer nanocomposite.

Here, we fabricated hyperbranched PU/SRGO (HPU/SRGO) nanocomposites with different weight% of SRGO. The mechanical properties, self-healing ability, shape memory behavior and antimicrobial properties of the nanocomposites were also delved into.

Experimental

Materials

Graphite flakes (60 meshes, purity 99%) and castor oil were obtained from Sigma-Aldrich, India. 1, 4-butanediol (BD) and sodium thiosulphate were purchased from Merck, India and used as received. Poly(ε-caprolactone) diol (PCL, Solvay Co., Mn= 3000 g mol-1) was also used as received. Lemon (Citrus limon) was collected from the local area. Monoglyceride of the castor oil was prepared as the previously reported[27] and GO was prepared according to modified Hummer's method.[34]

Preparation of SRGO nanohybrid

SRGO nanohybrid was prepared as reported in our earlier work.[35] Briefly, a thiosulfate solution was prepared by dissolving 64 mg of Na2S2O3 in 50 mL millipore water. Then 35 mL GO (1mg.mL-1) was added in to the solution and sonicated it for 30 min to obtain a GO dispersed thiosulfate solution. Then 10 mL of lemon juice was added into the solution and the mixture was stirred for 60 min under ambient condition to form the nanohybrid. This prepared nanohybrid, SRGO was sonicated for 10 min. The resulting suspension was washed by repeated centrifugation with millipore water and acetone. Then it was dried in an oven at 60°C.

Preparation of HPU/SRGO nanocomposite

The nanocomposite was prepared by *in-situ* polymerization technique in a three-necked round bottomed flask, equipped with a nitrogen gas inlet, a mechanical stirrer and a Teflon septum. PCL (0.002 mol, 6 g), BD (0.004 mol, 0.36 g) and dispersion of SRGO in DMAc (different weight%: 0.5, 1 and 2 with respect to total weight of nanocomposite) were taken in the flask with desired amount of xylene (maintaining solid content at 40%). After dissolving PCL, TDI (0.007 mol, 1.22 g) was dropwise added by a syringe into the reaction mixture at room temperature. Then the reaction was continued for 3h at a temperature of (70±2) ºC to obtain the desired viscous mass, which was treated as pre-polymer.

Then this pre-polymer was cooled to room temperature and monoglyceride of castor oil (0.002 mol, 0.74 g) as a triol was added into it with the required amount of TDI (0.002 mol, 0.35 g). The temperature was then raised to (110±2) ºC and continuously stirred for 2.5 h to complete the reaction as indicated by the absence of isocyanate band at 2270 cm-1 in the FTIR spectrum. HPU was also prepared without using SRGO. HPU with 0.5, 1 and 2 weight% of SRGO were encoded as HPU/SRGO0.5, HPU/SRGO1 and HPU/SRGO2 respectively.

Material characterization

FTIR spectra of HPU and its nanocomposites were taken by a Nicolet (Madison, USA) FTIR impact 410 spectrophotometer over the wavenumber range of 4000–400 cm^{-1} using KBr pellets. XRD was carried out at room temperature (ca. 25 °C) by a Rigaku X-ray diffractometer (Miniflex, UK) over the range of 2θ = 2–70° at scanning rate 2°/min. TGA was done by a thermal analyzer, TGA4000, Perkin Elmer, USA with a nitrogen flow rate of 30 mL/min at heating rate of 10 °C/min. Differential scanning calorimetry (DSC) was performed by DSC 6000, Perkin Elmer, USA at 2 °C min^{-1} heating rate under the nitrogen flow rate of 30 mL min-1 from -40 to 120 °C. The tensile strength and elongation at break were measured on rectangular strip with dimension 80 × 10 × 0.50 mm^3 by the help of the Universal Testing Machine (UTM), Jinan WDW 10, China with a 500 N load cell at crosshead speed of 20 mm/min. Tensile modulus of the sample are obtained from the slopes of the linear areas in the stress–strain curves and toughness of the sample are calculated by integrating the stress–strain curves. Whereas tensile strength is measured as the maximum stress withstand by the sample before rapture.

Shape memory test

To study the shape memory behaviour under MW and direct sunlight, the bending test was performed. The sample was folded in a ring form at 60 °C followed by quenching into an ice-salt bath for 5 min at -10 °C. Then the shape recovery of the nanocomposite films was achieved by exposing MW irradiation

of 360 W for 30-60 s and direct sunlight (11 am-2 pm, at Tezpur University campus, altitude: 26.63 °N 92.8 °E in the month of March at sunny days with average temperature: 32±1 °C and humidity: 70±1 %). The shape recovery was calculated using the following equation.

Shape recovery (%) = {(90-θ)/90} ×100 ---------- (1)

Where θ in degree denotes the angle between the tangential line at the midpoint of the sample and the line connecting the midpoint and the end of the curved samples.

Self-healing test

In order to evaluate healing performance, the above rectangular strips of nanocomposite were cut (10 × 0.2 × 0.015 mm^3 in dimension) in transverse direction by a razor blade and the cracked was healed by sunlight and MW, separately. Healing efficiency was calculated as the ratio of tensile strength values of the nanocomposites before to after healing. The tensile strengths of the pristine and the healed samples were measured by using the same UTM. Tensile strengths of pristine HPU and nanocomposites with different loadings of nanohybrid were measured for at least 5 samples in each case, before and after healing process. The optimal healing time for each case is defined as the shortest time required to achieve the best healing efficiency under the given conditions. For MW healing, a domestic MW oven (800 W) at operating frequency of 2.45 GHz and MW power of 360 W was used. Samples are placed in the middle position of the rotating disc on a glass plate inside the MW oven with a chamber of interior dimension of 20 × 19 × 14 cm^3. Sunlight healing was performed under direct sunlight (11 am-2 pm) at Tezpur University campus (altitude: 26.63 °N 92.8 °E) in the month of March at sunny days [average temperature (34±1 °C) and humidity (74±1 %), light intensity: 90,000-100,000 lux].

Antimicrobial activity

Microbial strains used for the study were *Staphylococcus aureus* (ATCC 11632), *Escherichia coli* (ATCC 10536) and *Candida albicans* (ATCC 10231).

Minimum inhibitory concentrations (MIC) were calculated for the nanomaterials and HPU as well as for the nanocomposites. Mirco-dilution technique was adopted for the assay.[36] *S. aureus* and *E. coli* were cultured in Nutrient Broth (NB, HiMedia, India) for 24 h at 37 °C. *C. albicans* was grown in Potato Dextrose Broth (PDB, HiMedia, India) for 48 h at 28 °C inside an incubator. Serial dilution was done for the samples (from stock solutions with concentration 30 mg/mL) using 1% dimethylsulfoxide (DMSO, HiMedia, India). Samples (100 µL) were incubated with the microbial cultures (100 µL) in 96 well plates at their specific concentrations. Streptomycin and nystatin (HiMedia, India) were taken as the positive controls. After incubation of 24 and 48 h respectively for bacteria and fungus, 40 µL of 3-(4,5-dimethylthiazol-2-yl)-2,5-diphenyltetrazolium bromide (MTT) was poured into each well. Change in color of the media to dark blue implicated the viable microbial cells, while no change in color indicated the death cell.

Further, microbial growth patterns were studied in presence of HPU and the nanocomposite films. Microbial cultures were taken in 15 mL test tubes, in presence of the films and incubated for specific time period. Growth was determined by recording their UV absorbance at 600 nm. Test tubes, without film were considered as control. Further, test tubes containing HPU are taken for comparative study. SEM image was taken for *E. coli* as a representative species to observe the fate of the films adhered bacteria.

Again, HPU and the nanocomposite films (1.5 cm×1.5 cm×0.3 mm) were laid on solidified agar plates, where inoculums of bacteria and fungus were spread with the help of a spreader. Plates were incubated at 24 and 48 h at 37 and 28 °C in an incubator. Microbial growth inhibition over the films was witnessed by capturing the photographs of the plates in a Nikon coolpix camera and analyzed visually.[37]

Results and discussion

Preparation

The HPU/SRGO nanocomposite was prepared by an in-situ A2+B3 technique using monoglyceride of castor oil as a branching moiety (triol) and SRGO as reinforcing nanomaterial. The key factors for the successful preparation of HPU nanocomposite are concentration of the reactants (especially branching moiety), addition rate of the triol moiety, reaction time and temperature.[38] In 1st step of the polymerization process, SRGO dispersion in DMAc was incorporated for providing a chance to react the nanohybrid with a few isocyanate terminated prepolymer chains. This provides strong interfacial interactions between HPU chains and the nanohybrid.[34] In the 2nd step of the reaction, addition of multifunctional moiety (monoglyceride) was done slowly in a very dilute solution (15% in xylene) to avoid gel formation. Also, reaction temperature was elevated gradually from room temperature to 110 °C.[38]

Characterization

FTIR spectra of HPU and its nanocomposite are shown in Fig. 1. The formation of urethane linkage in HPU and its nanocomposite are confirmed by the presence of characteristic bands for N-H deformation vibration (1070-1090 cm^{-1}), C-O stretching vibration (1150-1170 cm^{-1}), amide II (N-H bending vibration and C-N stretching vibration, 1560–1580 cm^{-1}), amide I (C=O stretching vibration 1675-1685 cm^{-1}), and 3430 cm^{-1} (O-H free and N-H stretching vibrations).[25,27] The increase in broadening of –OH band and shifting of C=O band to 1675 from 1685 cm^{-1} were observed with the increasing amount of SRGO in the nanocomposite.[30] This indicated the presence of interactions among polymer chains and SRGO, which are increased with the SRGO content.

In the XRD patterns of HPU and its nanocomposites, two distinct peaks at 2θ = 21.1° (corresponding to d-spacing of 0.419 nm) and 23.4° (corresponding to d-spacing of 0.381 nm) are found for the crystals of PCL moiety of HPU (Fig. 2).[39]

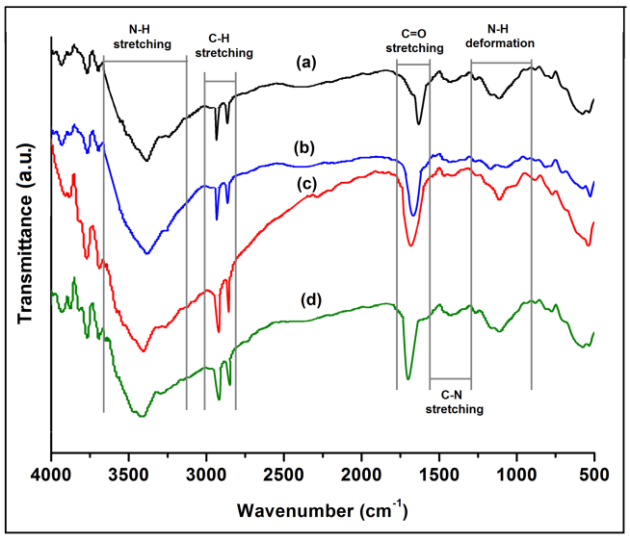

Fig. 1 FTIR spectra of (a) HPU, (b) HPU/SRGO0.5, (c) HPU/SRGO1 and (d) HPU/SRGO2.

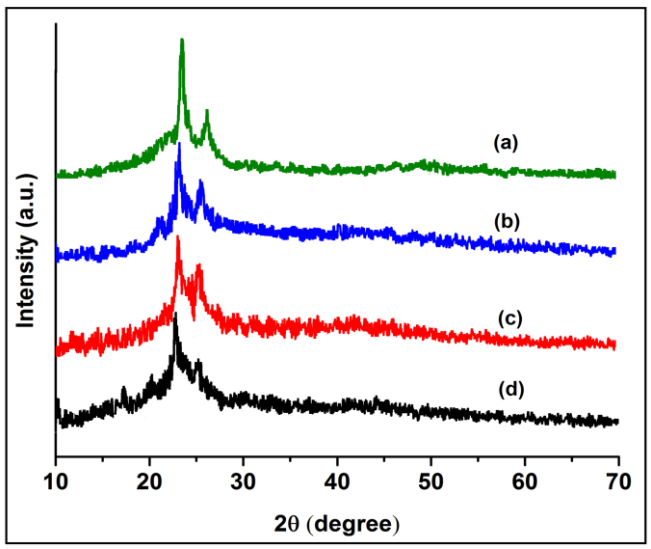

Fig. 2 XRD patterns of (a) HPU, (b) HPU/SRGO0.5, (c) HPU/SRGO1 and (d) HPU/SRGO2.

In the nanocomposites, minor shifting of PCL peaks towards higher angle were noticed due to formation of dense structure compared to pristine HPU.[26] Slightly increase in peak intensity of PCL moiety also found with increase in amount of SRGO due to nucleating effect of SRGO. Importantly, distinct peaks for SRGO are not found in the XRD patterns of nanocomposites as a small amount of SRGO is used to fabricate nanocomposite.[30]

Mechanical properties

The stress–strain profiles of neat HPU and its nanocomposites are shown in Fig. 3. The nanocomposite demonstrated extensive enhancement in mechanical properties after incorporation of a small amount of SRGO. Mechanical properties such as tensile strength, tensile modulus, elongation at break and toughness are summarized in Table 1. The

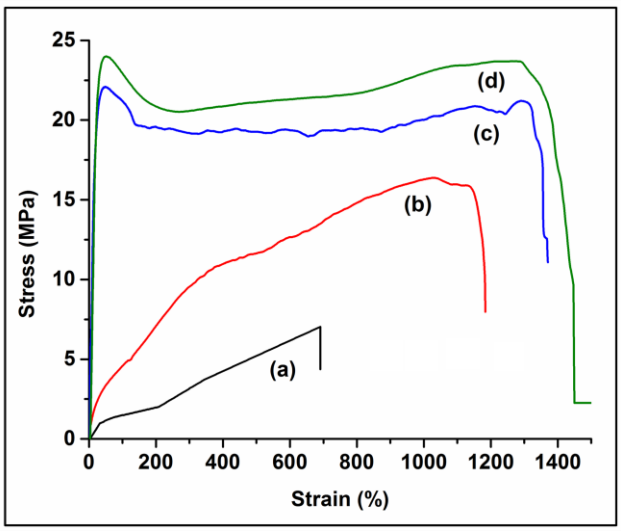

Fig. 3 Stress-strain profiles of (a) HPU, (b) HPU/SRGO0.5, (c) HPU/SRGO1 and (d) HPU/SRGO2.

presence strong interfacial interaction provided efficient load transfer ability between nanohybrid and polymer matrix.[26] These resulted in outstanding mechanical properties of the nanocomposite. Also due to formation of the covalent bond between prepolymer chains and functional groups of nanohybrid, hard segment of the HPU chains become stiff which results in high modulus and strength.[30] All the nanocomposite exhibited dose dependent mechanical properties. HPU and HPU/SRGO0.5 demonstrated typical elastomeric stress-strain profile, whereas HPU/SRGO1 and HPU/SRGO2 demonstrated typical flexible plastic stress-strain profile. From Fig. 3, it is also clear that tensile modulus and strength of nanocomposite are enhanced enormously in HPU/SRGO1 and HPU/SRGO2, compared to HPU/SRGO0.5. This indicated that small amount nanohybrid (0.5 weight %) do not establish appropriate interfaces and hence there might be a lack of load transfer from the polymer matrix to nanohybrid. This is directly reflected in low improvement in mechanical properties of HPU/SRGO0.5.

Toughness of the nanocomposite also enhanced with amount of nanohybrid and all the nanocomposite demonstrated excellent toughness compared to pristine HPU. Similar to our earlier report on graphene based nanocomposite, HPU/SRGO nanocomposite also exhibited higher elongation at break than pristine HPU and it is found to increase with the increase in nanohybrid content.[30]

Table 1 Mechanical properties of HPU and its nanocomposites

Sample	Tensile strength (MPa)	Tensile modulus (MPa)	Elongation at break (%)	Toughness (MJm^{-3})
HPU	7.2± 0.5	3.3± 0.2	710± 20	25.4± 1.2
HPU/SRGO 0.5	16.5± 0.7	13.6± 0.5	1186± 35	138.2± 2.2
HPU/SRGO 1	21.6± 1.1	130.64± 1.2	1372± 30	268.9± 3.4
HPU/SRGO 2	24.3± 1.3	137.74± 2.2	1456± 45	313.5± 4.3

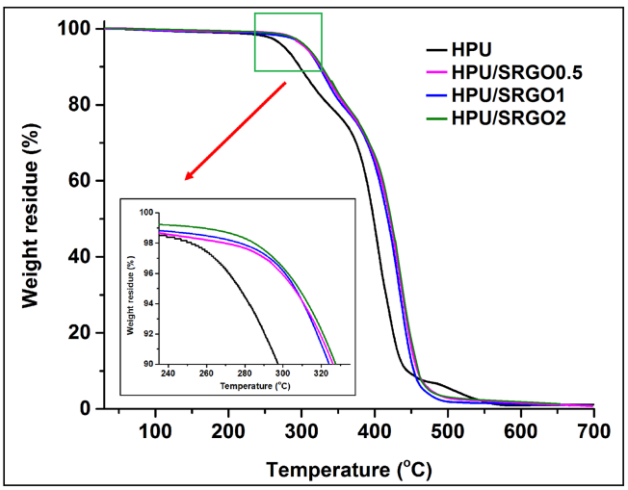

Fig. 4 TG thermograms of HPU and its nanocomposites.

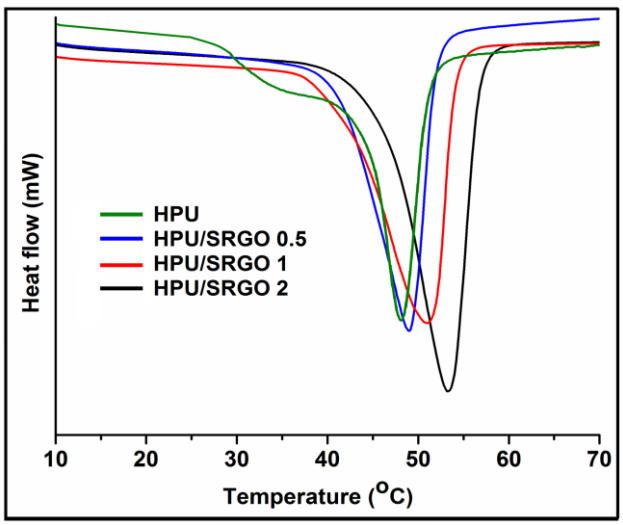

Fig. 5 DSC curves of HPU and its nanocomposites.

The enhancement of elongation at break is due to the alignment of polymer chains along the loading direction during the initial stress and sliding of layers of RGO at high stress. Elasto–plastic behavior of graphene sheets may also be another reason for it.[40]

Thermal properties

Thermal stability of the prepared nanocomposite are evaluated by thermogravimetric analysis and the thermograms are shown in Fig. 4. HPU and its nanocomposite show almost similar thermograms but nanocomposite demonstrate higher thermal stability compared to pristine HPU. From the thermograms, initial degradation temperature ($T_{initial}$) and midpoint degradation temperature (50% weight loss) are summarized in Table 2. The improvement in thermal stability of nanocomposite may be attributed to the so called ‘‘tortuous path’’ effect of RGO, which delays the escape of volatile degradation products and restricts the movement of polymeric

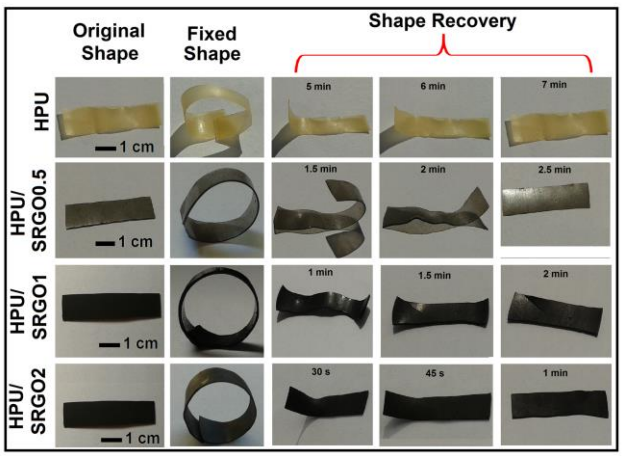

Fig.6 Shape memory behaviors of HPU and its nanocomposites under direct sunlight.

chains due to presence of strong interfacial interactions between HPU and nanohybrid.[41]

The degree of crystallinity and melting temperature (T_m) of the prepared nanocomposite were evaluated by DSC analysis (Fig. 5). The crystallinity found in the nanocomposite is due to presence of crystalline PCL moiety in the soft segment of HPU. The dose dependent degree of crystallinity and T_m values were observed for the nanocomposite with the content of nanohybrid (Table 2). These results are due to fact that the nanohybrid may help to orient the HPU chains in a particular direction and thereby restricting the mobility of the polymeric chains.

Shape memory behavior

Shape memory behaviours of HPU/SRGO nanocomposites under MW and sunlight are shown in Fig. 6. All the nanocomposites demonstrated excellent shape fixity and recovery under exposure of the mentioned stimuli. Shape recovery of the nanocomposite was faster and more efficient upon exposure to MW compared to sunlight. This may be due to excellent MW absorbing capacity of RGO than sunlight. Shape recovery time and ratio under different stimuli are tabulated in Table 3. The nanocomposite exhibited better shape recovery than HPU. Due to homogenous distribution of SRGO in the HPU matrix, high stored elastic strain energy is generated in the nanocomposite which helps the nanocomposites to achieve high recovery stress by releasing the stored elastic strain energy.[25,38] The shape recovery also found to be increased with increase in loading of nanohybrid.

Table 2 Thermal properties of HPU and its nanocomposites

Sample	$T_{initial}$ (°C)	Midpoint degradation temperature (°C)	Melting point of soft segment (°C)	Degree of crystallization (%)
HPU	277.23	398.41	48.4	27.62
HPU/SRGO 0.5	305.48	417.85	49.06	33.15
HPU/SRGO 1	306.71	420.39	51.12	35.14
HPU/SRGO 2	308.75	421.23	53.29	37.25

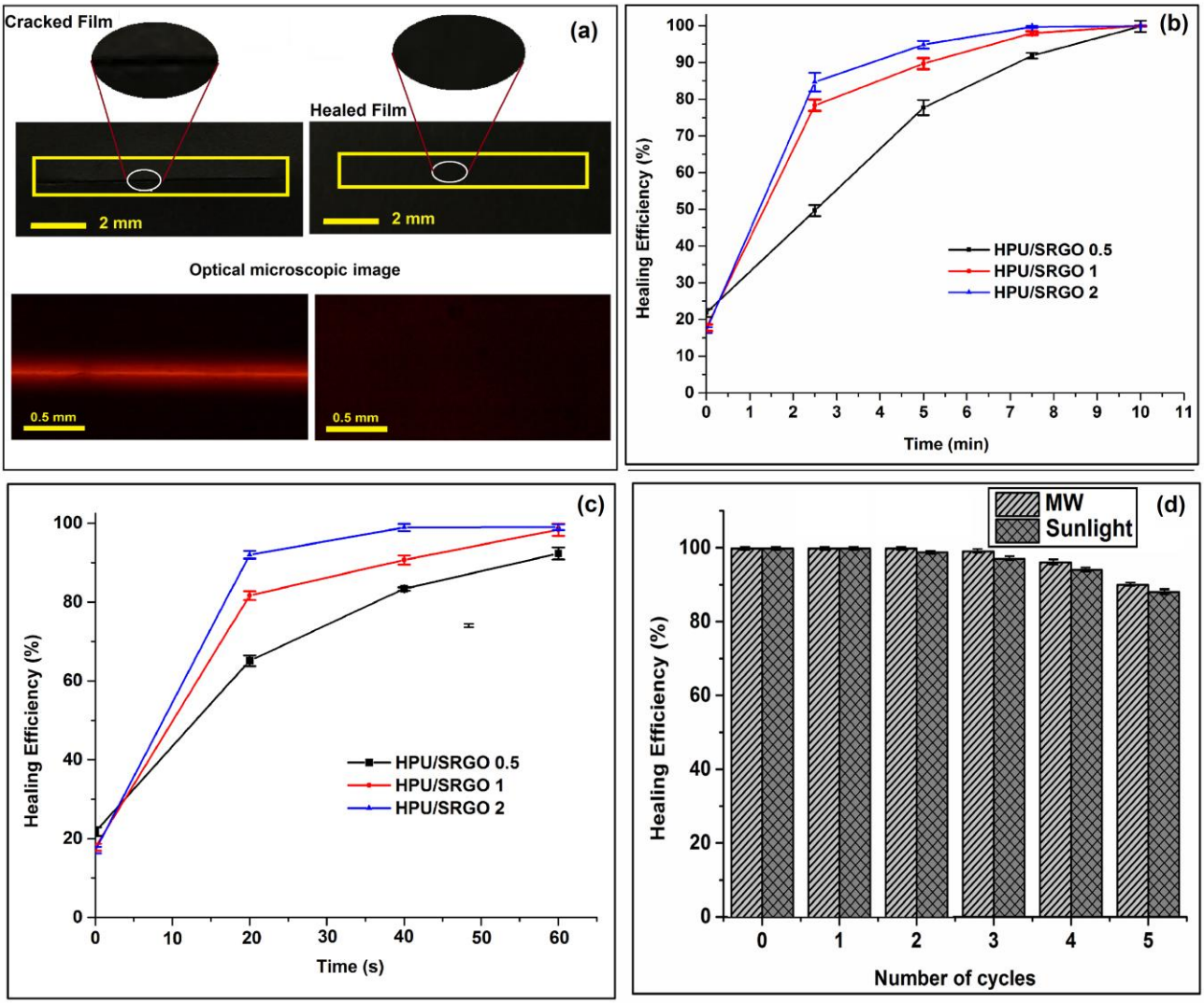

Fig. 7 (a) Digital and optical microscopic photographs of cracked and healed nanocomposite films; healing efficiency of the nanocomposites under (b) sunlight and (c) MW (360 W); and (d) repeatable healing efficiency of the nanocomposite under sunlight and MW.

More amount of unlocked oriented chains are generated owing to increase in crystallinity of the nanocomposite on incorporation of nanohybrid (as obtained from DSC and XRD results). These unlocked chains can produce an instantaneous retractive force upon elimination of the load because of the elastic entropy and hence it improved the shape recovery.

Self-healing properties

Tensile tests and optical images were used to examine the self-healing behavior of the nanocomposite. Fracture of the nanocomposite is effectively healed by exposure of direct sunlight and MW as shown in Fig. 7. Healing efficiency of nanocomposite under sunlight and MW are shown in the Fig. 7. Healing efficiency of the nanocomposite depends on loading of SRGO, power input of MW and exposure time (Fig. 8). In this context, it is pertinent to mention that pristine HPU does not heal upon exposure of different stimuli even after long time. All the nanocomposites were effectively healed within 30-50 s under low MW power (360W) and within 5-7.5 min under direct sunlight. During the healing process, SRGO absorbed energy from the stimulus and then transferred this energy to the HPU matrix.

Table 3 Shape memory properties of the nanocomposites

Stimulus	HPU		HPU/SRGO 0.5		HPU/SRGO 1		HPU/SRGO 2	
	Shape recovery time	Shape recovery (%)	Shape recovery time	Shape recovery (%)	Shape recovery time	Shape recovery (%)	Shape recovery time	Shape recovery (%)
MW	80 ± 2 s	95.4 ± 0.2	70 ± 2 s	96.8 ± 0.1	60 ± 2 s	97.6 ± 0.2	45 ± 2 s	98.6 ± 0.1
Sunlight	7 ± 0.5 min	95.7 ± 0.1	2.5 ± 0.2 min	96.2 ± 0.1	2 ± 0. 3 min	97.4 ± 0.2	1± 0.1 min	98.5 ± 0.1

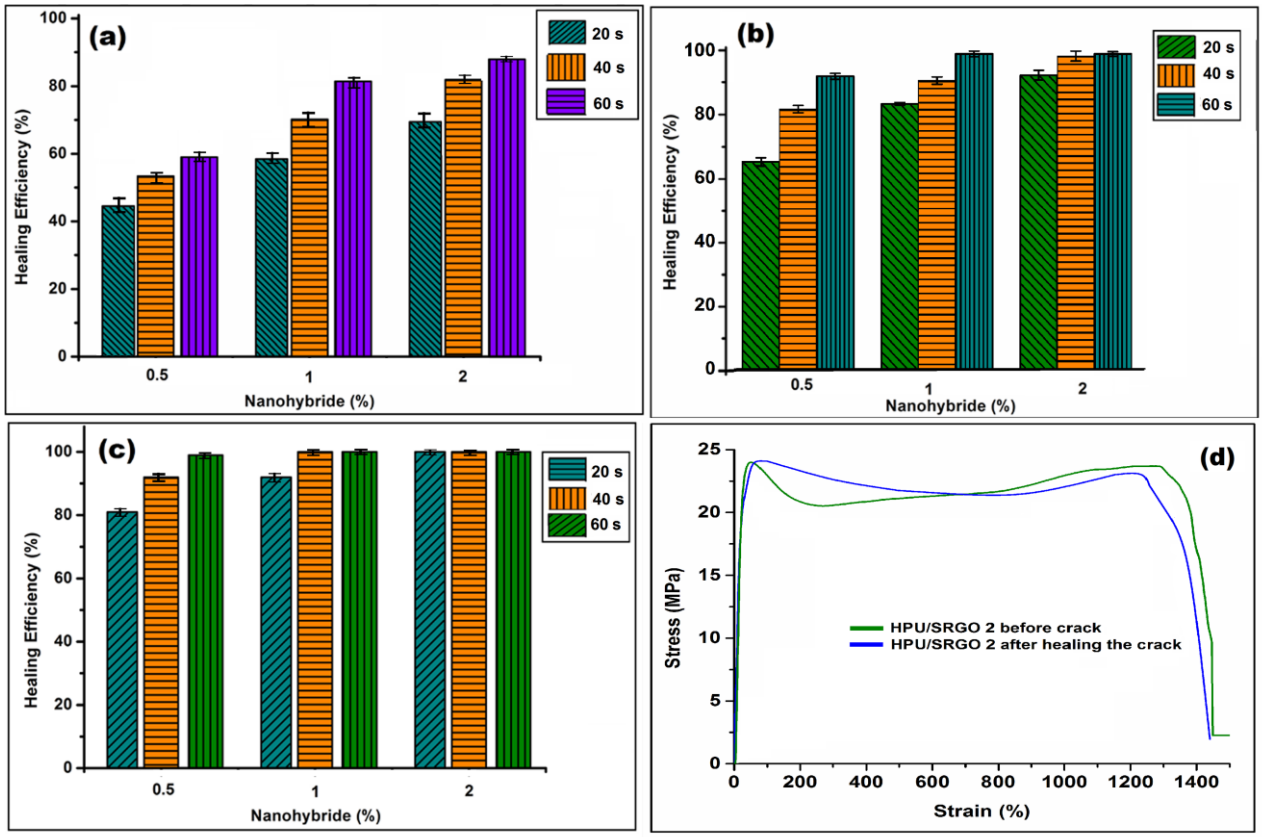

Fig. 8 The healing efficiency of the nanocomposite at different MW power input of (a) 180 W, (b) 360 W and (c) 540 W; and (d) representative stress-strain curves of HPU/SRGO 2 before crack and after healing the crack.

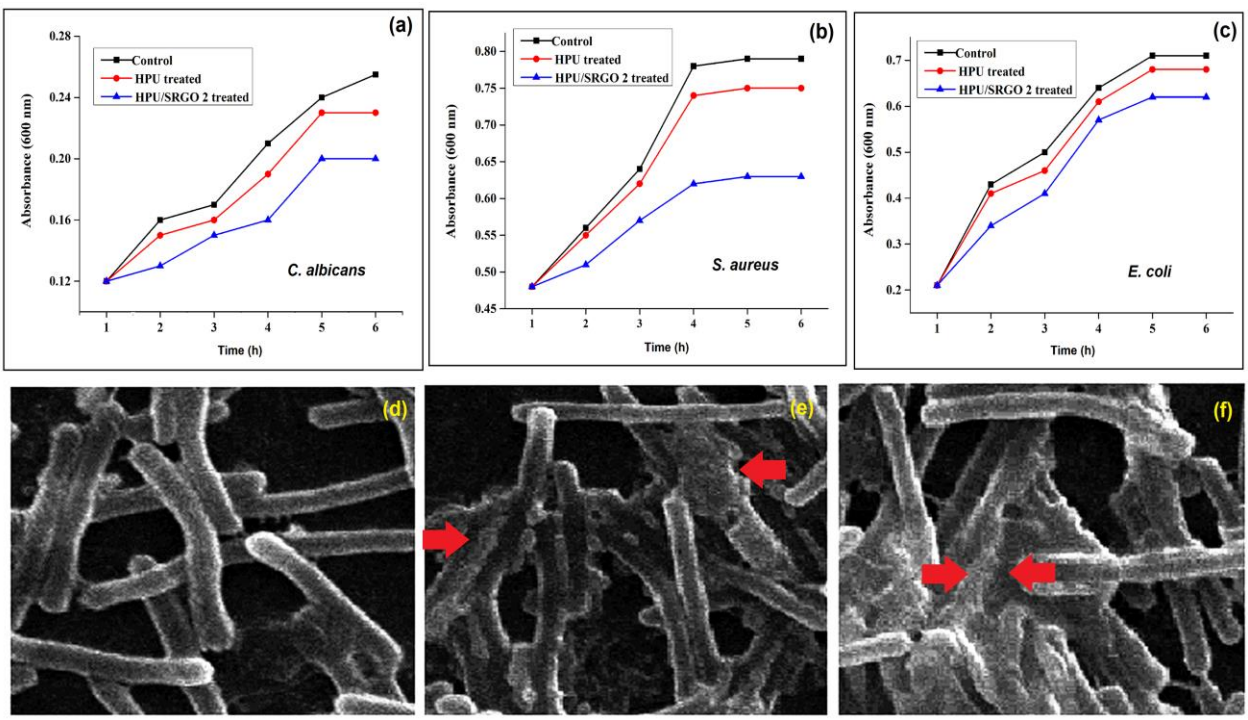

Fig. 9 MIC of nanocomposite against (a) *Candida ablicans*, (b) *Escherichia coli*, (c) *Staphylococcus aureus*; and SEM image of *E. coli* cells adhered to (d) HPU, (e) HPU/RGO and (f) HPU/SRGO.

The soft segment of the HPU is melted by gaining the energy as it Tm is around 50 °C. So the crack could repair with a higher mobility of soft segment of HPU. At the same time, hard segment of HPU helps to keep its original shape. The shape memory properties of nanocomposite also played a vital role in the healing process.[17] When energy is transfered to HPU chains by SRGO, it activated and then the internal stress was released. Therefore, notch's surface of the crack was firstly healed with the help of the recovery force from the bottom before complete repairing of the crack.[18] Here it is important to notice that HPU shows a SME but not self-healing ability although both the process depend on rearrangement of the polymeric chains. As, the energy requirement to activate the polymeric chain for rearranging its orientation and gaining its original shape is less compared to diffuse the polymeric chains in the crack site. A huge amount energy is needed to melt a particular segment of the polymer and subsequent diffusion. Pristine HPU has only polar group which are only capable to absorb some energy from the stimulus for rearranging them and return from a deformed state (temporary shape) to their original (permanent) shape. But this much of energy may not be sufficient for polymeric chains diffusion and as result pristine HPU only demonstrates SME. In contrast to that SRGO nanohybrid has a good capability to absorb energy from MW and sunlight and hence SRGO absorb and transfer more amount of the energy to HPU matrix of the nanocomposite. Therefore, soft segment of HPU is melted in the nanocomposite and diffused in crack place to heal it.

Repeated healing is a daunting challenge to the material scientist and important for the self-healing materials which could greatly increase the service lifetime. In our work, self-healing was achieved by the rearrangement of soft segments of HPU with the assistance of the SME, so the healing of the prepared nanocomposite could be repeated again and again. Thus, even after fifth cycle of experiment, the healing ability of the nanocomposite remains almost same under both sunlight and MW (Fig. 7).

Antimicrobial activity

SRGO exhibited the lowest MIC against both bacteria and fungus (Table 4). As sulfur nanoparticles and RGO showed strong antimicrobial effect so the nanohybrid demonstrated a synergistic effect against the tested microbes. However, indirect contact of SRGO with the microbial strains suppressed the inhibitory action in case of nanocomposite. Thus, a high dose of the nanocomposite was required to show the inhibitory effect. MIC values suggest that the nanocomposite can inhibit both Gram positive and negative bacteria; though the effect is more pronounced for the former. Contrarily, HPU exhibited inhibitory effect at very high dose, which implicates that SRGO is mainly responsible for conferring antimicrobial efficacy to the nanocomposites. Antifungal activity of the nanohybrid, as well as nanocomposite was also found to be significantly effective. However, in each case, declination of growth was seen when incubated with HPU/SRGO2 films. Statistical measurements (Two way ANOVA) revealed that

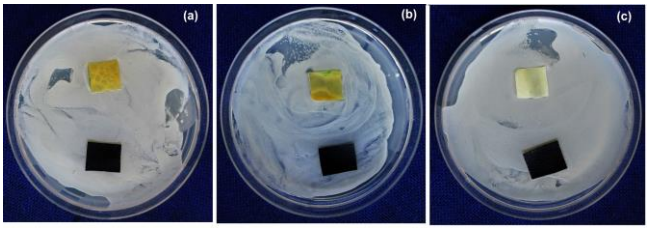

Fig. 10 Growth of (a) *Staphylococcus aureus*, (b) *Escherichia coli* and (c) *Candida albicans* in close proximity of HPU/SRGO.

the MIC values were significantly different from each other, with LSD 0.63 and $p<0.05$.

It is clearly visible from Fig 9 (a-c) that microbial growth increased exponentially with time in the controls. On the other hand, presence of HPU/SRGO2 inhibited the growth rate of each microbe, considered under the test. Another, interesting conclusion derived from the assay is that growth rate of the strains are not much hampered by the presence of HPU. This again validates the efficient antimicrobial activity of SRGO. Microorganism, adhering on antimicrobial surfaces, lost their morphological integrity.[42] Cell membrane lysis is the vital factor for the decrement of growth rate. To ascertain this, *E. coli* was considered as a representative microbe for SEM analysis. From Fig. 9 (d-f) it is observed that membrane disruption occurred in the bacterial cells that attached to HPU/SRGO2 surface. Red marks indicated the irregularity in the cellular structures and agglomeration of the dead cells. However, bacteria attached to HPU surface did not lose their cellular structure. This confirmed the microbial growth resisting potential of HPU/SRGO2. This antimicrobial property is very useful to fabricate various advanced materials which could be able to prevent microbial contamination and infections.

Another assay was performed to verify the possibility of microbial growth, in the proximity of HPU and HPU/SRGO2. Thus, images were taken and analyzed for the films, laid in petri plates with each of the test microorganism (Fig. 10). Images confirmed that none of the microbes could grow over HPU/SRGO 2 surface within an area of 1.5 cm^2, while significant growth was witnessed over the surface of HPU. This implicated that the nanocomposite did not allow microbial fouling over its surface, even in close contact with them. The overall study endorse the material as an advance antimicrobial nanocomposite with high mechanical attributes.

Table 4 MIC against bacteria and fungus

Microbe	HPU (μg/ml)	RGO (μg/ml)	Sulfur nanoparticles (μg/ml)	SRGO (μg/ml)	HPUSRGO (μg/ml)
S. aureus	180± 2.6	22.7± 1.57	18.3±0.57	13.7± 1.50	33.7± 1.52
E. coli	245 ± 3.2	31.0± 1.00	21.7±1.52	19.3± 0.57	43.0± 2.00
C. albicans	272 ± 3.6	47.0± 1.00	33.7±1.50	29.0± 1.00	63.3± 1.52

Conclusions

In summary, we developed a tough HPU/SRGO nanocomposite which demonstrated excellent self-healing and shape recovery with significant antimicrobial activity. The nanocomposite exhibited improved mechanical and thermal properties after incorporation of a small amount of nanohybrid owing to good interaction between nanohybrid and HPU. The nanocomposite also showed excellent rapid and repeatable self-healing and shape recovery by MW and sunlight. The presence of SRGO nanohybrid in nanocomposite provided good antimicrobial activity against gram positive and negative bacteria along with fungus. Thus, the multifunctional smart nanocomposite has great potential in domain of advanced material.

Acknowledgements

S.T. sincerely acknowledges the receipt of his Senior Research Fellowship from the Council of Scientific and Industrial Research (CSIR), India. The authors express their gratitude to SAP (UGC), India through grant No. F.3-30/2009(SAP-II) and FIST program-2009 (DST), India through the grant No.SR/FST/CSI-203/209/1 dated 06.05.2010.

Notes and references

Advanced Polymer and Nanomaterial Laboratory, Department of Chemical Sciences (Centre for Polymer Science and Technology), Tezpur University, Tezpur 784028, India.
Fax: +91 3712-267006; Tel: +91 3712-267327;
E-mail: karakniranjan@gmail.com (N. Karak)

1. S. D. Bergman and F. Wudl, *J. Mater. Chem.* 2008, **18**, 41-62.
2. M. Nosonovsky, R. Amano, J. M. Lucci and P. K. Rohatgi, *Phys. Chem. Chem. Phys.* 2009, **11**, 9530-9536.
3. X. J. Ye, J. L. Zhang, Y. Zhu, M. Z. Rong, M. Q. Zhang, Y. X. Song and H. X. Zhang, *ACS Appl. Mater. Interfaces* 2014, **6** (5), 3661–3670.
4. X. Wang, Y. Wang, S. Bi, Y. Wang, X. Chen, L. Qiu and J. Sun, *Adv. Funct. Mater*. 2014, **24**, 403–411.
5. R. Jones, A. Cintora, S. R. White and N. R. Sottos, *ACS Appl. Mater. Interfaces*, 2014, **6** (9), 6033–6039.
6. X. M. Na, F. Gao, L. Y. Zhang, Z. G. Su and G. H. Ma, *ACS Macro Lett.* 2012, **1**, 697–700.
7. P. M. Imbesi, C. Fidge, J. E. Raymond, S. I. Cauet and K. L. Wooley, *ACS Macro Lett.* 2012, **1,** 473– 477.
8. Y. X. Lu and Z. Guan, *J. Am. Chem. Soc.* 2012, **134**, 14226–14231.
9. S. R. White, N. R. Sottos, P. H. Geubelle, J. S. Moore, M. R Kessler, S. R. Sriram, E. N. Brown and S. Viswanathan. *Nature* 2001, **409**, 794-797.
10. H. Jin, C. L. Mangun, A. S. Griffin, J. S. Moore, N. R. Sottos and S. R. White, *Adv. Mater*. 2014, **26**, 282-287.
11. H. Jin, C. L. Mangun, D. S. Stradley, J. S. Moore, N. R. Sottos and S. R. White, *Polymer* 2012, **53**, 581-587.
12. G. Wu, J. An, X-Z. Tang, Y. Xiang and J. Yang, *Adv. Funct. Mater*. doi: 10.1002/adfm.201401473.
13. H. Zhang, P. Wang and J. Yang, *Compos. Sci. Technol.* 2014, **94,** 23-29.
14. E. L. Kirkby, V. J. Michaud, J-A. Månson, N. R. Sottos and S. R. White, *Polymer* 2009, **50**, 5533-5538.
15. E. L. Kirkby, J. D. Rule, V. J. Michaud, N. R. Sottos, S. R. White and J.-A. E. Månson, *Adv. Funct. Mater.* 2008, **18**, 2253–2260.
16. B. T. Michal, C. A. Jaye, E. J. Spencer and S. J. Rowan, *ACS Macro Lett.* 2013, **2**, 694–699.
17. X. Wang, J. Zhao, M. Chen, L. Ma, X. Zhao, Z. M. Dang and Z. Wang, *J. Phys. Chem. B* 2013, **117**, 1467–1474.
18. Y. Bai, Y. Chen, Q. Wang and T. Wang, *J. Mater. Chem. A* 2014, **2**, 9169-9177.
19. Q. L. Zhang, S. J. Song, J. C. Feng and P. Y. Wu, *J. Mater. Chem.* 2012, **22**, 24776–24782.
20. Y. C. Jung, H. J. Yoo, Y. A. Kim, J. W. Cho and M. Endo, *Carbon* 2010, **48**, 1598–1603.
21. U. N. Kumar, K. Kratz, M. Heuchel, M. Behl and A. Lendlein, *Adv. Mater*. 2011, **23**, 4157–4162.
22. H. Zhang, J. Zhang, X. Tong, D. Ma and Y. Zhao, *Macromol. Rapid Commun.* 2013, **34**, 1575–1579.
23. J. Hu, Y. Zhu, H. Huang and J. Lu, *Prog. Polym. Sci.* 2012, **37**, 1720–1763.
24. J. Leng, X. Lan, Y. Liu and S. Du, *Prog. Mater. Sci.* 2011, **56**, 1077–1135.
25. S. Thakur and N. Karak, *RSC Adv*. 2013, **3**, 9476–9482.
26. K. M. S. Meera, R. M. Sankar, J. Paul, S. N. Jaisankar and A. B. Mandal, *Phys. Chem. Chem. Phys.*, 2014, **16**, 9276-9288.
27. S. Thakur and N. Karak, *Prog. Org. Coat*. 2013, **76**, 157–164.
28. B. Voit, *J. Polym. Sci. Part A: Polym. Chem*. 2005, **43**, 2679–2699.
29. L. Huang, N. Yi, Y. Wu, Y. Zhang, Q. Zhang, Y. Huang, Y. Ma and Y. Chen, *Adv. Mater*. 2013, **25**, 2224–2228.
30. S. Thakur and N. Karak, *ACS Sustainable Chem. Eng.* 2014, **2**, 1195−1202.
31. S. Liu, T. H. Zeng, M. Hofmann, E. Burcombe, J. Wei, R. Jiang, J. Kong and Y. Chen, *ACS Nano* 2011, **5** (9) 6971– 6980.
32. T. Schneider, A. Baldauf, L. A. Ba, V. Jamier, K. Khairan, M. B. Sarakbi, N. Reum, M. Schneider, A. Röseler, O. Burkholz, P. G. Winyard, M. Kelkel, M. Diederich, K. Becker and C. Jacob, *J. Biomed. Nanotechnol.* 2011, **7**, 395-405.
33. H. Kalita, M. Mandal and N. Karak, *J. Polym. Res*. 2012, **19**, 9982.
34. S. Thakur and N. Karak, *Carbon* 2012, **50**, 5331-5339.
35. S. Thakur, G. das, P. K. Raul and N. Karak, *J. Phys. Chem. C* 2013, **117**, 7636–7642.
36. S. Barua, S. Thakur, L. Aidew, A.K. Buragohain, P. Chattopadhyay and N. Karak, *RSC Adv.* 2014, **4** (19), 9777-9783.
37. S. Barua, P. Chattopadhyay, M. M Phukan, B. K Konwar and N. Karak, *Mater. Res. Express* 2014, **1**, 045402.
38. S. Thakur and N. Karak, *J. Mater. Chem. A*, 2014, **2**, 14867-14875.
39. H. Kalita and N. Karak, *Polym. Adv. Technol*. 2013, **24**, 819–823.
40. H. J. Yoo, S. S. Mahapatra and J. W. Cho, *J. Phys. Chem. C* 2014, **118** (19), 10408–10415.
41. X. Wang, Y. Hu, L. Song, H. Yang, W. Xing and H. Lu, *J. Mater. Chem.* 2011, **21**, 4222-4227.
42. M. L. W. Knetsch and L. H. Koole, *Polymers* 2011, **3**, 340-366.